

JAXA-ONERA-DLR COOPERATION: RESULTS FROM ROTOR OPTIMIZATION IN FORWARD FLIGHT

Keita Kimura, keita.kimura@jaxa.jp, Japan Aerospace Exploration Agency/JAXA (Japan)
 Gunther Wilke, gunther.wilke@dlr.de, German Aerospace Center/DLR (Germany)
 Joëlle Bailly, joelle.zibi@onera.fr, The French Aerospace Lab/ONERA (France)
 Yasutada Tanabe, tan@chofu.jaxa.jp, Japan Aerospace Exploration Agency/JAXA (Japan)

Abstract

This paper presents the results of a cooperative study by JAXA, DLR, and ONERA on the optimal design of helicopter blades for high-speed forward flight. Optimizations and simulations are carried out by each agency with their own analysis codes using both blade element theory-based methods and computational fluid dynamics. These results are cross-compared and show common trends identified for optimum rotor blades obtained by each agency and the mechanism for improving forward flight performance are discussed. From the effective drag distributions, it is confirmed that, in order to improve forward flight performance, it is first important to reduce drag on the advancing side, and that a blade with a relatively small twist angle and planforms with a smaller chord length at the root and tip compared to the mid-span section is generally a suitable blade.

1. INTRODUCTION

JAXA, ONERA, and DLR have independently been working to establish rotor blade optimization methodologies [1] [2] [3]. In 2019, the three organizations agreed to collaborate on a joint research project in order to cross-validate and accumulate knowledge of optimization methods and performance evaluation tools for helicopter main rotor blades through common case studies.

In Phase I of this collaboration, low-fidelity and CFD based methods have been compared with respect to their ability to reflect geometrical changes of the blades as well as their potential to further optimize blades. [4]

In Phase II of the optimization cooperation, the blade optimization for a high-speed forward flight condition is studied. Recently, the development of compound helicopters has been gaining momentum worldwide, with the development of aircraft such as Airbus' RACER [5] and Sikorsky's Raider/SB-1 Defiant [6] which are capable of flying in excess of 400 km/h. This is a significant increase in speed compared to existing helicopters, which had a cruising speed of around 200 km/h and requires a different blade shape design.

Therefore, in recent years, one design issue has been the blade optimum design technique for high-speed flight, for example, there are previous studies that described the blade design philosophy of the Sikorsky X2 [7] and confirmed the effect of twist distribution on the forward flight performance of a wing-type compound helicopter [8].

This study investigates the effect of different distributions of chord length and twist angle on the rotor performance. It aims to accumulate knowledge on the reasonable setting of design variables and optimization procedures.

2. METHODOLOGY

2.1. Simulation Approach

2.1.1 Low-Fidelity Setups

The underlying methodology used for the low-fidelity aerodynamics is the blade-element theory (BET). The sectional forces of the rotor blades are determined from look-up tables of the airfoils. The main differences lie in the inflow model used by the partners. JAXA utilizes the momentum theory (BEMT), while DLR and ONERA utilized prescribed wake model by [9] of the comprehensive code HOST [12].

Table 1 Low-fidelity method to evaluate rotor performance

| | JAXA | ONERA | DLR |
|-----------------------|--------------|-----------------|-----------------------------|
| code | rBET | HOST [12] | |
| Inflow model | Pitt & Peter | Prescribed wake | |
| Structural adjustment | - | Polynomial fit | Stanger monocoque type [13] |

2.1.2 Computational Fluid Dynamics

All three partner have their each own structured codes for the simulation of the rotor blades. For brevity, the major features are compared in Table 2. For more information for each solver, please consult the associated references. For details of grid setting, refer to [4] for setting up.

In JAXA's simulations, rectangular background grids are prepared and a set of overlapping blade grids is placed within them. The calculation proceeds by moving this blade grid at each calculation step. Pointwise was used to create the blade grid, and rGrid, an automatic mesher provided by JAXA, is used to generate the background grids.

ONERA takes a similar approach for JAXA, but uses a chimera technique to model a single rotor blade within a quarter cylinder. A multi-block, deformable mesh of O-H type is generated for the blade mesh, where the root and tip caps are

modelled in separate grid blocks. The grids of the new rotor designs are generated through a deformation of the baseline grid, based on a quaternion approach, developed in the in-house QUANTUM code. The background grid is automatically generated using Cassiopee, a set of Python modules for pre- and post-processing of CFD computations.

DLR uses their own grid generator G³(G-cube) based on transfinite interpolation, like GEROS [14]. Thus, a grid is automatically generated for each new rotor design. Here an O-O block is generated with periodic boundaries, which is extended by additional H-O blocks towards the farfield. Like ONERA, the Froude boundary condition is available on the outer mesh. This mesh is referred to as "monocoque", since it does not rely on the Chimera/Overset technique. For the later side studies, an additional Chimera setup is also prepared with the in-house grid generator and referred to as "chimera".

Table 2 : High-fidelity method to evaluate rotor performance

| | JAXA | ONERA | DLR |
|------------------|---|---|--|
| solver | rFlow3D [15] | e/sA [16] | FLOWer [17] |
| Inviscid scheme | 4 th order FMCT [18]+SLAU2 [19] | 2 nd order JST [20] | 4 th order FMCT [18] (vA) [21]+SLAU2 [19] |
| | with 2 nd order finite volume metrics | | |
| Time integration | Dual time LU-SGS (Blade) [22] & 4 stage RK (Background) | Dual time Backward Euler scheme + LU-SSOR [23] | Dual time Backward Euler scheme + LU-SGS [22] |
| Turb. model | SA [24]-R [25] Fully turbulent | Kok-SST [26] Fully turbulent | SA [24] DDES [27] R [25] + empirical transition [28] |
| Rotor property | Rigid | Elastic, through delta airloads approach with HOST [12] | |

2.2. Optimization Setup

2.2.1 Optimization Framework

The general optimization approach for this work is based on the EGO optimization algorithm by Jones et al. [29]. A Kriging surrogate model is built after an initial data sampling and the next infill point is sought using the maximum expected improvement. However, variations in the implemented frameworks exist and are listed in Table 3.

The low-fidelity optimizations are purely carried out with the standard Kriging model. For the high-

fidelity optimizations, ONERA and DLR make use of the variable-fidelity approach, where the Kriging model is augmented with high-fidelity data. ONERA utilizes the low-fidelity model based on the finite-state inflow for Kriging combined with high fidelity data obtained from CFD/CSD coupling for Co-Kriging. DLR generates CFD data using a factor eight coarsened grid and Hierarchical Kriging.

Table 3 : Optimization frameworks

| | JAXA | ONERA | DLR |
|------------|-------------------|--------------|--------------------------------|
| Frame-work | - | KORRIGAN [3] | POT [2] |
| Meta model | Kriging | Co-Kriging | Hierarchical Kriging |
| Optimizer | Genetic Algorithm | | Diff. Evolution +Nelder & Mead |

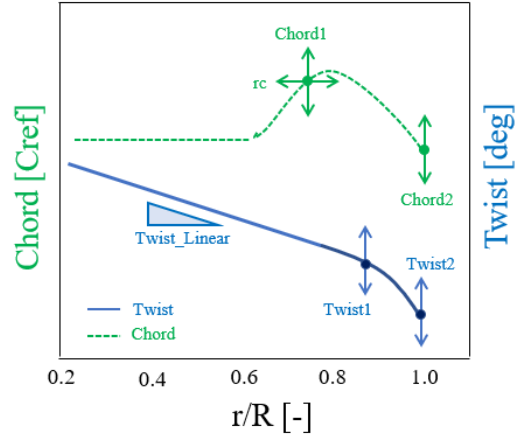


Figure 1 : Sketch of design variables

2.2.2 Design variables and Goal Function

To efficiently optimize the blade shape, it is essential to appropriately set fewer design variables to describe the twist and chord where the sensitivity onto the performance is large. A total of six variables is applied, three for twist, and three for the chord length distribution, see Figure 1 to get how to work each design variables.

Table 4. By adding the constraint that the thrust weighted equivalent chord length c_{ref} (eq.1) is constant, the chord length at the root is indirectly varied according to the settings of dv4 and dv5 (chord lengths near the blade tip). In eq. (1), c is the chord length at radial position r and R is the blade radius.

$$(1) \quad c_{ref} = \frac{\int_0^R c(r)r^2 dr}{\int_0^R r^2 dr}$$

Table 4 : Design variables

| Name | Variables setting | Range |
|--------------|---|-------------|
| Twist1 | dθ1 @r/R = 0.875 | -5°~5° |
| Twist2 | dθ2 @r/R = 1.0 | -5°~5° |
| Twist Linear | Linear nose down twist from root to tip | -10°~0° |
| rc | control section for chord1 | 0.5R~0.85R |
| Chord1 | Chord @rc | 1.0~1.5Cref |
| Chord2 | Chord @r/R = 1.0 | 0.5~1.0Cref |

The proposed metric for the rotor blade performance is the effective lift-drag ratio L/D_e or the effective drag D_e which represents the forward flight efficiency. The definition of L/D_e is expressed as follows, where L is the rotor lift, D is the wind-axis drag force, P is the power of rotor and Q is the rotor torque. V_∞ and V_{tip} represent the flight speed and tip-speed.

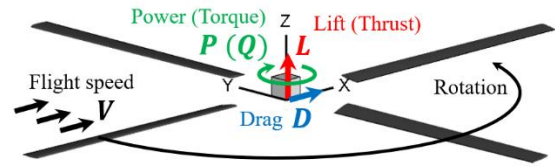


Figure 2 : Aerodynamic components to be considered for calculate the goal function (effective lift to drag ratio L/D_e)

$$(2) \quad C_T = \frac{L}{\rho AV_{tip}^2} \quad C_D = \frac{D}{\rho AV_{tip}^2}$$

$$C_Q = \frac{Q}{\rho AV_{tip}^2 R} \quad C_P = \frac{P}{\rho AV_{tip}^3}$$

$$\mu = \frac{V_\infty}{V_{tip}}$$

$$C_{De} = C_D + C_Q/\mu$$

$$(3) \quad L/D_e = \frac{C_T}{C_D + C_Q/\mu} = \frac{C_T}{C_{De}}$$

2.2.3 Flight Conditions

The flight condition to be optimized (Table 5) and the baseline blade specifications (Table 6) are explained here. The optimization assumes a compound helicopter with a separate lift generator, such as a fixed-wing, and the main rotor is set to generate a lift corresponding to 30% of the aircraft's weight. To achieve a high advance ratio, the main rotor in this setup is rotated at a lower speed compared to the blade tip speed of conventional helicopters. The shaft axis is set at 0° shaft angle to keep the rotor disk horizontal and reduce rotor drag during high-speed flight. The baseline rotor chosen here is the HARTII rotor [30]. It has a rectangular blade with a linear nose-down twist.

Table 5 : Flight condition

| item | Value |
|------------------|------------------------|
| Thrust | 1080 [N] (30% of lift) |
| CT/σ | 0.034 (σ = 0.077) |
| Advance ratio | 0.7 |
| Minf | 0.34 |
| Mtip | 0.48 |
| Rotational speed | 781.5 [RPM] |
| Shaft angle | 0 [°] |

Table 6 : specification of baseline blade (HARTII blade)

| item | Value |
|------------------------|-------------|
| # of blades | 4 |
| Radius | 2 [m] |
| Cref | 0.121 [m] |
| Linear nose-down twist | -8 [°] |
| shape | Rectangular |
| Airfoil | NACA23012 |

3. RESULTS

3.1. Baseline case comparison

To confirm the accuracy of the forward flight performance analysis for each agency, trim analyses are performed on the baseline blade (HARTII) using the low-fidelity and high-fidelity methods under the conditions shown in Table 5. Figure 3 and Figure 4 show the effective drag and the pitch angle history calculated by low-fidelity methods for each partner. The pitch angle history has a very large variation and a difference of about

6 deg exists for both collective and cyclic pitch. The definition of pitch angle is as follows (4)

$$(4) \quad \theta = \theta_0 + \theta_{1c} \cos \psi + \theta_{1s} \sin \psi$$

where θ_0 is the collective pitch and θ_{1c} and θ_{1s} are the lateral and longitudinal cyclic pitch angle respectively. ψ is the azimuth angle and takes values up to 360° counterclockwise with 0° behind the rotor

It should be due to the fidelity of the induced flow model considered, and JAXA, which employs a simple linear model, shows very small pitch angles. On the other hand, DLR and ONERA, which are given more reproducible induction velocities by the prescribe wake model, show results of several degs in collective/cyclic pitch angles.

While the pitch angle range varied widely, it should be noted that JAXA's results are not significantly different from those of DLR/ONERA when compared in terms of effective drag. The results of the low-fidelity method for all five cases showed that the largest variation in effective drag is in the DNERA rigid case and the DLR soft case, where the difference is about 16%.

In addition, a comparison of the ONERA and DLR results between the soft case, which takes elastic deformation into account, and the rigid case, which assumes a rigid body, confirmed a tendency for the C_D value to increase and the C_Q value to decrease when the case is changed from rigid to soft. This suggests that wind axis drag is increasing on the retracted side of the rotor. This is because the wind axis force (drag) applied to the rotor on the retreating side means that the force is applied in the direction to rotate the rotor, resulting in a smaller torque.

Similarly, Figure 5 and Figure 6 show the results of the high-fidelity methods, comparing the data while keeping in mind that only JAXA assumes a rigid body blade, it seems that the induced velocity distribution on the rotor surface is more directly linked to the collective/cyclic pitch values than in the low-fidelity method, where the induced flow distribution is arbitrary. Compared to the low-fidelity method, the pitch angle values appear to be more directly reflected in the rotor performance. The JAXA and DLR results with similar pitch angle behavior show good effective drag agreement, while the ONERA results with half the value of the longitudinal cyclic pitch show relatively large values for both C_D and C_Q .

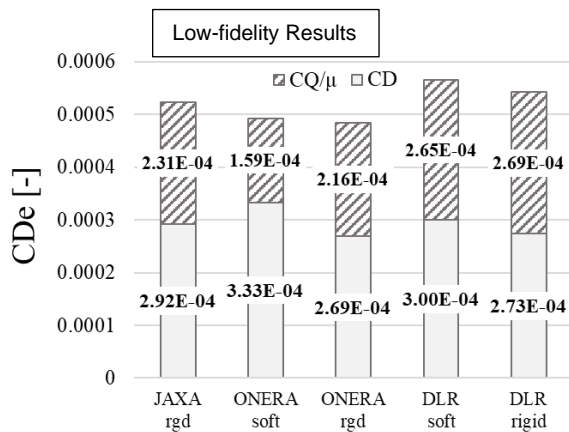


Figure 3 : Effective drag of Baseline blade (HARTII) each shape optimized by low-fidelity methods

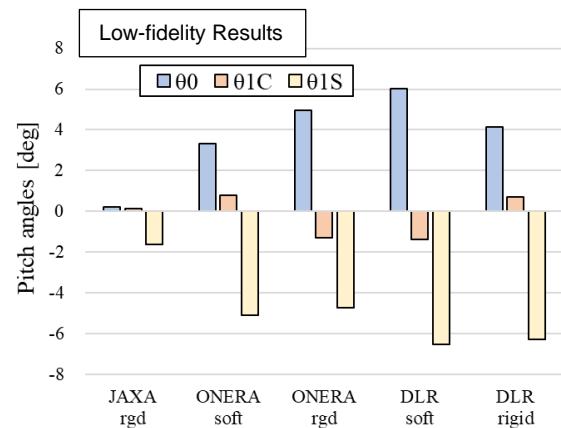


Figure 4 : Pitch controls for Baseline blade (HARTII) by low-fidelity methods

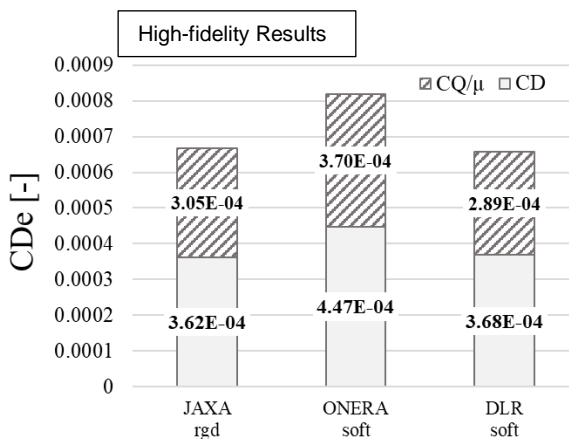


Figure 5 : Effective drag of Baseline blade (HARTII) each shape optimized by high-fidelity methods

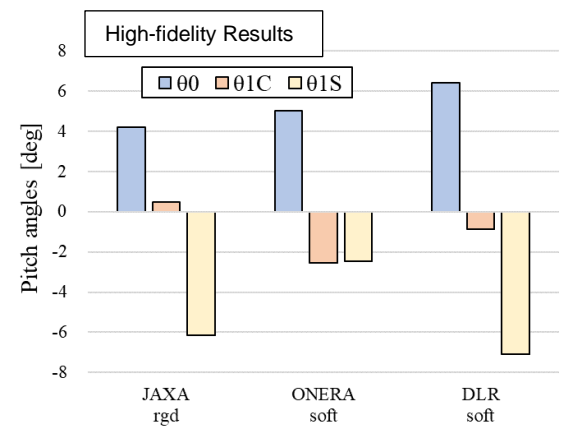


Figure 6 : Pitch controls for Baseline blade (HARTII) by high-fidelity methods

3.2. Obtained shapes

The geometry obtained by optimization is shown in Figure 7. Several variations exist depending on the analysis tools used by each partner and whether or not the elasticity of the blades is considered. As a general trend of the planform, the chord length at the mid-span tends to be larger, while the chord length at the blade root and tip tends to be smaller. For reference, the hovering-optimal rotor blades had a shape with a large chord length at the blade root and tapering toward the tip. Different shapes are obtained by changing the mission to be optimized.

In the following sections, the shapes obtained with low-fidelity and high-fidelity are shown, respectively. Figure 7 shows the parameters of each blade.



Figure 7 : Planforms obtained by optimization

Table 7 : Design variables for each optimum shape

| | Twist1 | Twist2 | Linear-Twist | rc | Chord 1 | Chord 2 |
|----|--------|--------|--------------|------|---------|---------|
| D1 | -0.151 | 0.590 | -4.47 | 0.85 | 1.5 | 0.5 |
| D2 | 0.501 | -0.620 | -3.41 | 0.85 | 1.5 | 0.5 |
| D3 | -0.171 | 1.022 | -0.868 | 0.5 | 1.5 | 1.0 |
| O1 | 1.59 | -0.152 | -5.36 | 0.5 | 1.5 | 1.0 |
| O2 | 0.105 | -0.05 | -2.35 | 0.85 | 1.5 | 0.5 |
| J1 | 0.717 | 0.368 | -2.70 | 0.51 | 1.47 | 1.0 |
| J2 | -0.629 | 0.170 | -3.40 | 0.50 | 1.47 | 0.91 |

*D = DLR, O = ONERA, J = JAXA. See Figure 7 for details

3.2.1 Low-fidelity optimization

Figure 8 and Figure 9 show chord and twist distributions. The HARTII shape, which is the baseline shape, is shown together for reference. As for the chord distribution, the major trend is that the chord at midsection is larger, as mentioned earlier, and the chord lengths at the blade root and tip are smaller due to the constraint of constant equivalent chord. For the twist angle distribution, modifications were made in the direction of approaching a smaller, flatter blade compared to the baseline.

In addition, there is a difference in the position of the peak chord length between the rigid and elastic blade analysis conditions. When optimization is performed considering elastic deformation, the blade root is thickened and the peak position of the chord length is also sharpened while moving closer to the blade edge. It can be considered that the blade has evolved to reduce twist deformation by securing the chord length at the root, so as not to cause deterioration of rotor performance.

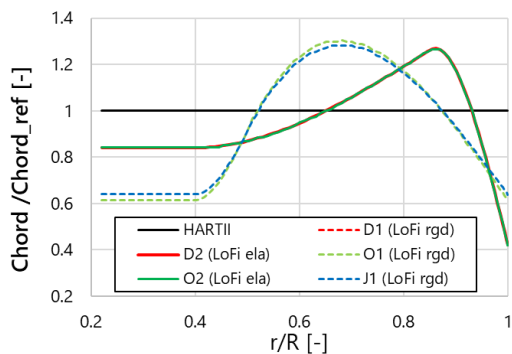


Figure 8 : chord distribution (LoFi optimized shapes)

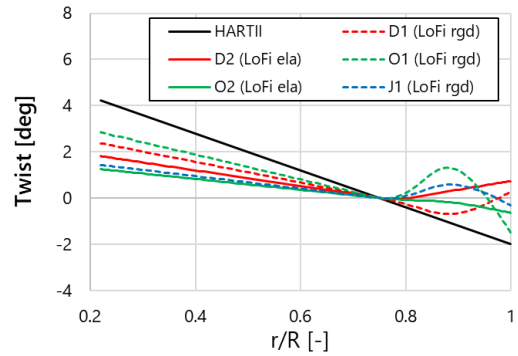


Figure 9 : twist distribution (LoFi optimized shapes)

3.2.2 Hi-fi optimization

Then similarly, the chord lengths and twist distributions are shown in and for the shapes obtained by the high-fidelity method (CFD). Shown here are the two optimal blades J2 under the rigid assumption of JAXA and D3 considering the structural deformation of the DLR. Despite these different assumptions, unlike the low-fidelity case, the chord length distribution is almost identical. While the difference in linear twist value is large.

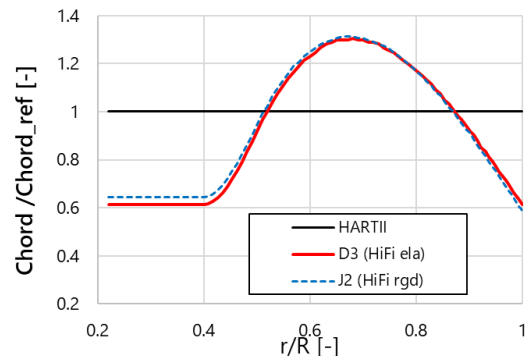


Figure 10 : chord distribution (HiFi optimized shapes)

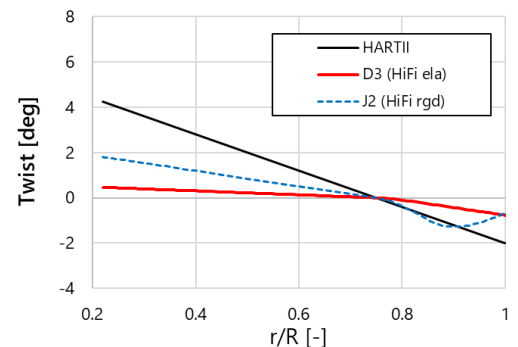


Figure 11 : twist distribution (LoFi optimized shapes)

3.3. Performance

Next, the forward flight performances of each blade are evaluated using the low-fidelity/high-fidelity method.

Figure 12 and Figure 13 summarize the results of the low-fidelity method and they are color-coded by institution. The effective drag is lower for the obtained blades compared to the Baseline (BLN) results, indicating that the optimization improves

performance. Comparison of effective lift-drag ratios shows that JAXA has improved performance by about 20% from BLN to J1 blades, ONERA by 12% from BLN to O1 blades, and DLR by about 18% from BLN to D2 blades.

Similarly, in the high-fidelity case (Figure 14 and Figure 15), the variance was even smaller in terms of the percentage of performance improvement observed at each organization, with forward flight performance improvements of 14% at JAXA, 17% at ONERA, and 16% at DLR.

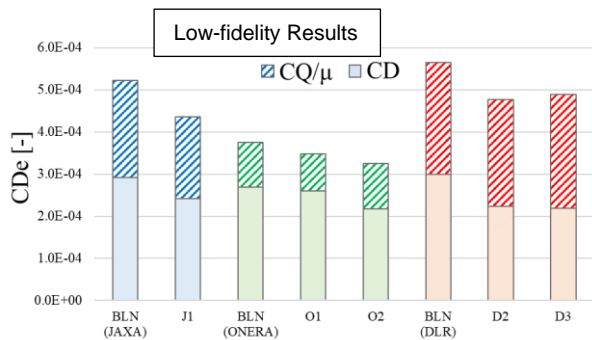


Figure 12 : Effective drag of each shape optimized by low-fidelity methods (Color-coded by partner where analysis was performed)

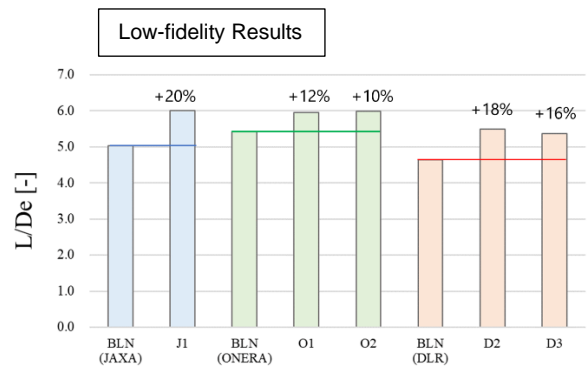


Figure 13 : Effective lift to drag ratio of shapes optimized by low-fidelity methods

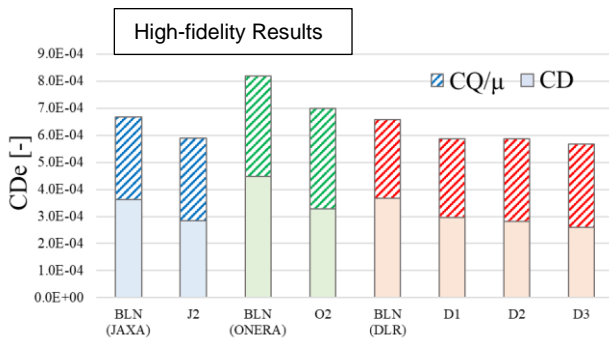


Figure 14 : Effective drag of each shape optimized by high-fidelity methods (Color-coded by partner where analysis was performed)

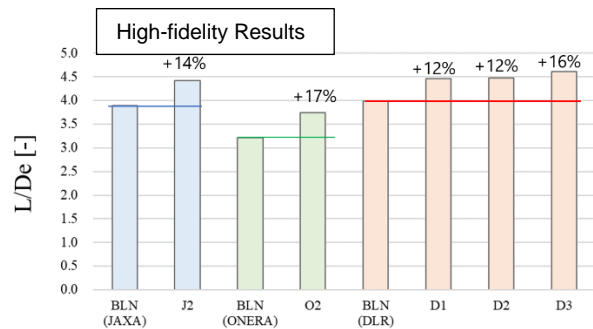


Figure 15 : Effective lift to drag ratio of shapes optimized by high-fidelity methods

The pitch angle histories of the rotor blades for the low-fidelity and high-fidelity method analyses are displayed in Figure 16 and Figure 17.

Compared to hovering, which theoretically does not require cyclic pitch control, the introduction of the

uncertainty of longitudinal and lateral cyclic control have caused the variability in results.

First, as a basic matter, the dynamic pressure received by the blade during forward flight is greater on the forward side, where the blade moves

toward the relative wind due to forward flight, and smaller on the backward side, where the blade moves away. Therefore, to balance the rolling moment, pitch-down control is applied on the advancing side (around $\psi=90^\circ$) and pitch-up control is applied on the retreating side (around $\psi=270^\circ$). This should be universally true for high advance ratio rotors, and the trend is confirmed in both low-fidelity and high-fidelity, and in all partners results, although the values are small and large.

The pitch angle history of the baseline blades is drawn as dashed lines and that of the optimal designed blades as solid lines. This is thought to be due to the fact that the optimal blades have a smaller twist angle and therefore require larger pitching motion than the baseline blades in order to create a large angle of attack in the reverse flow region.

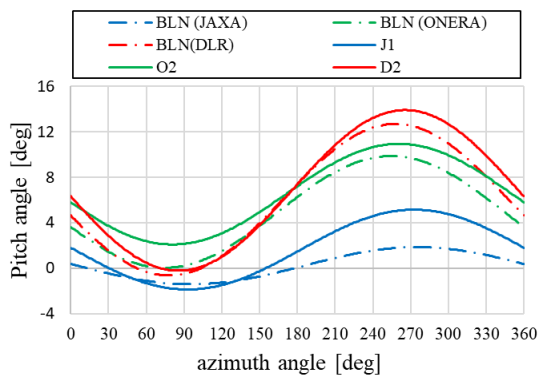


Figure 16 : Pitch angle history (Low-fidelity method)

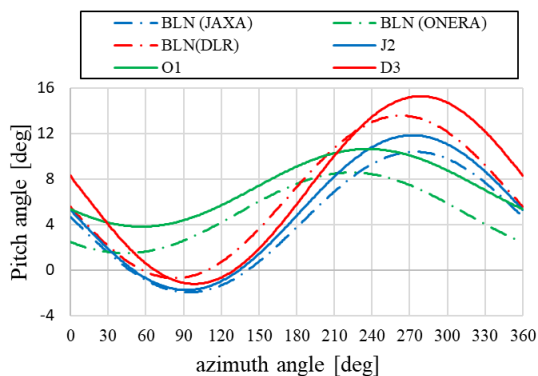


Figure 17 : Pitch angle history (High-fidelity method)

4. DISCUSSION

4.1. Azimuthal distribution

One of the characteristic aerodynamic features of a helicopter in forward flight is the asymmetry between the advancing and retreating sides. The relative velocities that the blades are subjected to on the advancing and retreating sides of the fuselage are quite different, therefore naturally the effect of optimization is expected to vary from azimuth to azimuth. Figure 18 shows the distribution of aerodynamic forces (three components: Thrust, drag, and Torque) at each azimuthal angle ($\psi=0\sim 360^\circ$). The results are obtained using the high-fidelity method for the baseline (HARTII) blades and the optimal blades for each partner. A common feature of the Baseline blade results is the large variation seen on the forward side ($0\sim 180^\circ$). In particular, all three partners show sharp fluctuations around $\psi=90^\circ$, where the dynamic pressure acting on the blade tip is the largest, and this is the peak position of negative lift. This is a trend that is more noticeable in rotors in high advance ratio conditions. If a large lift would be generated on the advancing side, a large rolling moment would be applied, and it would hard to compensate for this on the retreating side, where the dynamic pressure is small and the reverse flow area is mostly occupied. The elasticity-aware ONERA and DLR results matched very well, with a tendency for smaller fluctuations when optimized, while JAXA blades analyzed under rigid conditions tended to exhibit greater negative lift.

Drag and torque, which are effective drag components, are also notably high on the advancing side, suggesting that it is important to reduce them at advancing-side by optimization.

It should also be noted that when considering the relationship between drag and torque, it is difficult to reduce the effective drag on the retreating-side due to its mechanism. It is a fact that drag (F_x) on the retreating side is a force acting in the direction of turning the rotor blades, and thus acting in the direction of reducing the rotor torque.

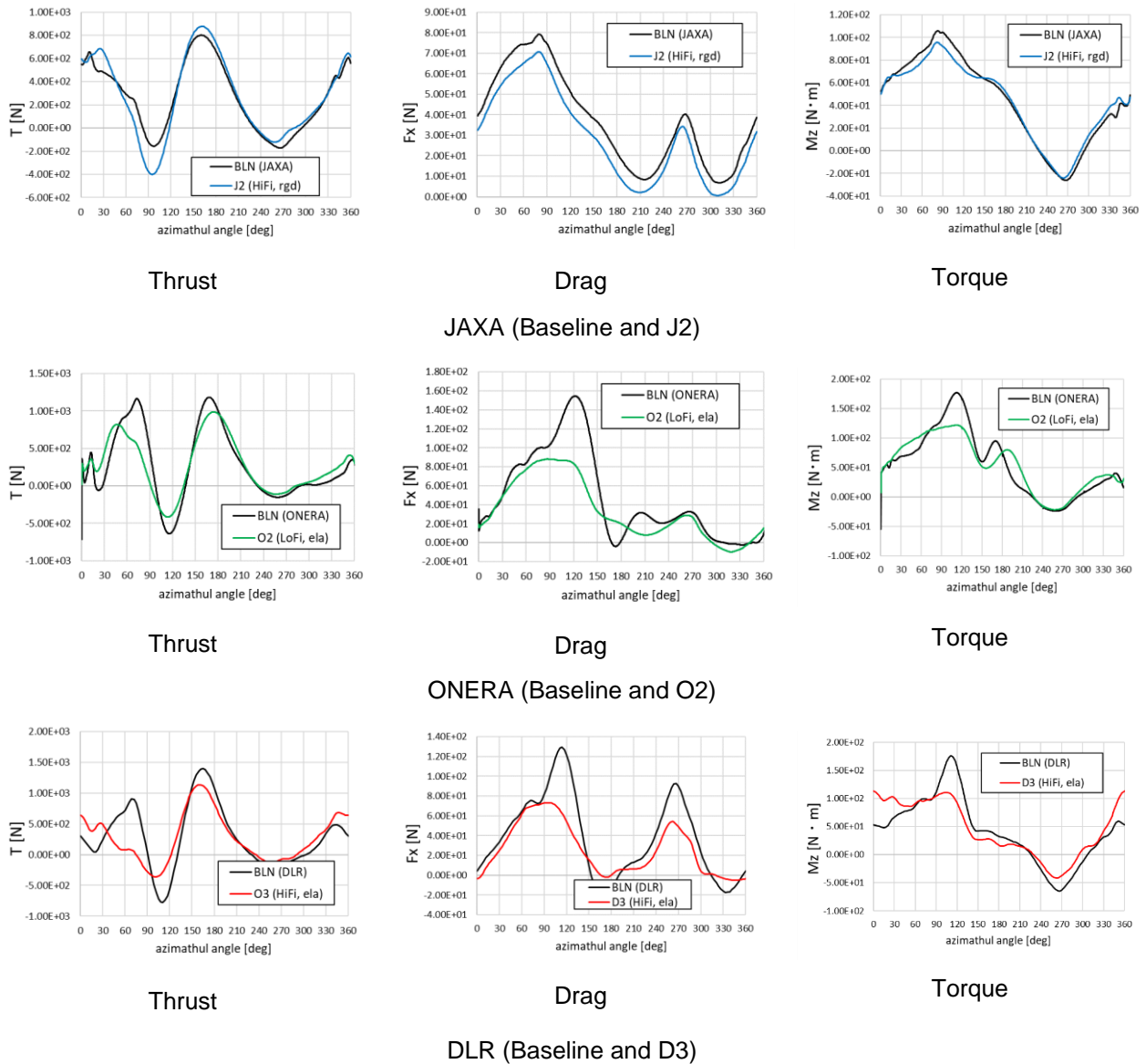


Figure 18 : Aerodynamic components at each azimuthal angle (integrated value over blade span at each azimuth)

4.2. Disk Distribution

To examine the aerodynamic design requirements, visualize the distribution on the rotor disk and check the distribution of thrust and drag. Figure 19 provides an overview of the method used to create the disk distribution. For a blade, the aerodynamic distribution for each azimuthal angle and each span position is collected and displayed in the form of a disk. The aerodynamic forces are visualized according to equations (4) and (5), where the contribution of lift and effective drag is large.

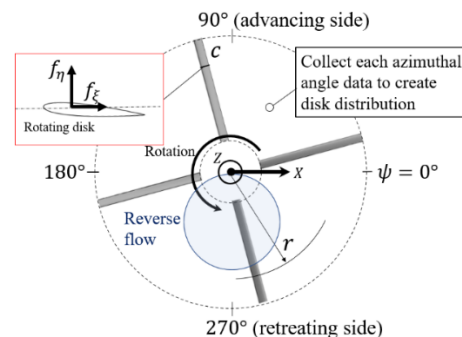


Figure 19 : How to calculate disk distribution

$$(5) \quad C_z M^2 = \frac{f_\eta}{\frac{1}{2} \rho a_\infty^2 c}$$

$$(6) \quad C_{De} M^2 = C_D M^2 + C_Q M^2 / \mu$$

$$C_D M^2 = \frac{f_\xi \sin \psi}{\frac{1}{2} \rho a_\infty^2 c} \quad C_Q M^2 = \frac{f_\xi r}{\frac{1}{2} \rho a_\infty^2 c R}$$

Figure 20 shows the lift coefficient distribution ($C_z M^2$). The comparison between the baseline and the optimum shapes shows that the lift generated around the tip of the advancing-side is reduced, and the lift distribution at the front and aft positions of the rotor-disk is increased to compensate for the reduction. Rotor blades for each of the three engines are considered to have evolved in a rational manner. Since a rotor in forward flight experience left-right imbalance, it is more convenient from the perspective of maintaining the aircraft's attitude when the lift force is carried by the front and rear of the rotor disk, considering the balance of rolling moment.

In addition, by reviewing the distribution of effective drag coefficients in

Figure 21, one can see how localized the distribution of drag sources is. It can be understood that most of them are on the advancing side and near the blade tips.

With respect to the reverse flow region, which was intuitively considered to be a major source of drag, the contribution varied from institution to institution.

For example, ONERA results show that the effective drag in the reverse flow region is negative especially around blade root, on the other hand positive for the DLR results. The trend is likely to change with the size of the trim angle, however in any case, the area that is likely to be a large source of drag is a limited compared to the advancing side.

However, as mentioned in Section 4.1, since the contribution of effective drag on the retreating side is not dominant, the possibility of this difference making a significant impact on performance is not great. On the other hand, in the advancing-side, reducing wind axis drag is directly related to decreasing rotor torque, which is significant from the standpoint of improving rotor performance.

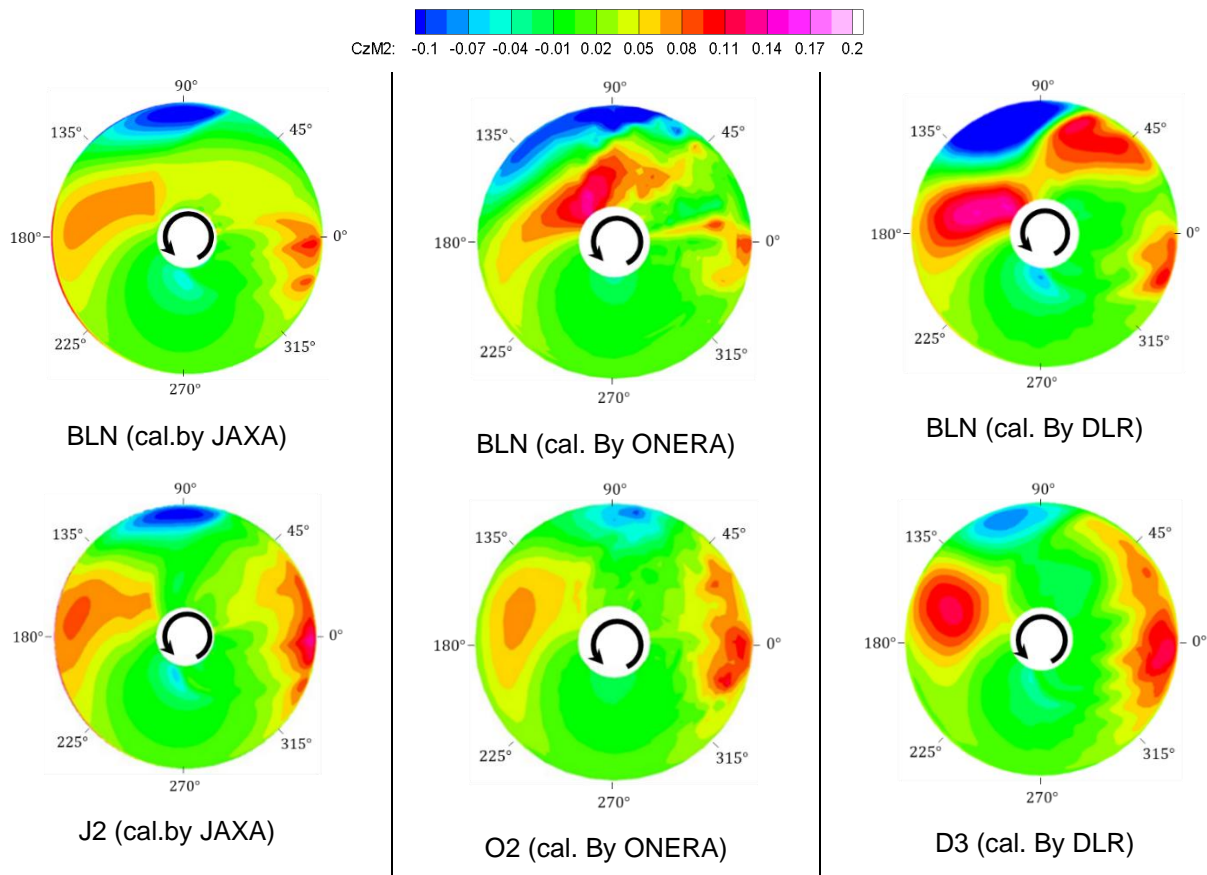


Figure 20 : Thrust ($C_z M^2$) distribution on the rotor disk

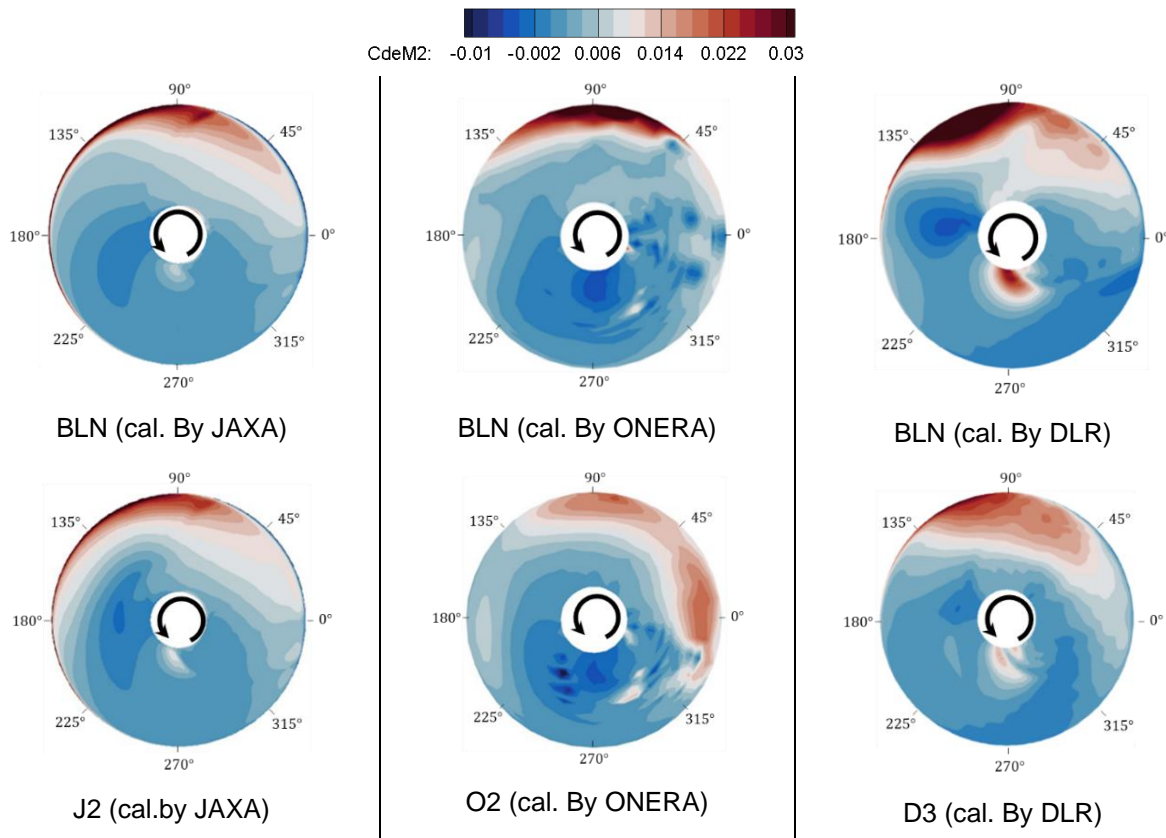


Figure 21 : Effective drag ($C_{De}M^2$) distribution on the rotor disk

5. CONCLUSION

Optimization of high-speed forward flight performance is conducted as Phase II of a cooperative study of optimal design methods for helicopter rotor blades between JAXA, DLR and ONERA. A HARTII blade is selected as the baseline blade, and a high advance ratio condition of $\mu=0.7$ is used, a value that assumes a future high-speed helicopter mission. The findings and a summary of the results are presented below.

- The three partners performed forward flight analyses of baseline blade (HARTII) using low-fidelity method based on blade element theory and CFD owned by each organization and compared effective drag and pitch angle. In the low-fidelity method, the pitch angle history differed greatly depending on the inflow model, while the effective drag values are similar among the three partners. In the CFD analysis, the pitch angle history is directly reflected in the induce flow, and the correlation between the pitch angle history and the effective drag is confirmed.

- Blade optimization using six design variables: two points for the twist angle around the blade tip, two of the chord length (plus one is the spanwise position specifying the chord length), and the linear twist value, resulted in a blade that is expected to improve forward flight performance by 10 to 20% for each agency.

- All three agencies found a common design trends that a design with a smaller twist angle is better compared to the baseline blade. For blades with large twist angles, it is difficult to reduce wind axis drag by control the pitch angle, therefore it is the result of optimization to avoid this.

- In blade optimization for high-speed forward flight conditions, it is most important to reduce wind axis drag on the advancing side of the rotor, especially at blade tip. This is because the dynamic pressure is the largest, and a reduction in wind axis drag directly leads to a reduction in rotor torque. In blades that achieve this, the thrust and drag on the left/right sides of the rotor are lowered and instead generated in front and aft of the rotor.

- Reducing drag in the reverse-flow region is effective in terms of performance improvement, however priority should be given to reducing drag

at the blade tips of the advancing-side blades, where dynamic pressure is large.

- One of the reasons why it is difficult to reduce the effective drag on the retreating side ($\psi = 180\sim 360$ deg) is that drag(=F_x) in this region acts as negative torque (in the direction that rotates the rotor), so in principle, rotor drag and torque cannot be reduced simultaneously.

6. REFERENCE

- [1] M. Sugiura, Y. Tanabe, H. Sugawara, K. Takekawa, "Optimal Design of Rotor Blade for a Winged Compound Helicopter at High Advance Ratio," in Proceedings of the 76th VFS Annual Forum, Virtual, 2020.
- [2] G. Wilke, "Variable-Fidelity Methodology for the Aerodynamic Optimization of Helicopter Rotors," vol.57, p.3145-3158, 2019.
- [3] J. Bailly, D. Bailly, "Multifidelity Aerodynamic Optimization of a Helicopter Rotor Blade," AIAA Journal, Vol.57, p.3132-3144, 2019.
- [4] G. Wilke, J. Bailly, K. Kimura, Y. Tanabe, "JAXA-ONERA-DLR cooperation: results from rotor optimization in hover," CEAS Aeronautical Journal, 13(2), 313-333, 2021.
- [5] "RACER -An aerodynamic configuration at the service of high speed-," AIRBUS, [Online]. Available: <https://www.airbus.com/en/innovation/disruptive-concepts/disruptive-design/racer>. [Accessed 22 8 2022].
- [6] "RAIDERX/DEFIANTX HP," LOCKHEED MARTIN, [Online]. Available: <https://www.lockheedmartin.com/fvl/index.html>. [Accessed 22 8 2022].
- [7] A. Bagai, "Aerodynamic design of the X2 technology demonstrator™ main rotor blade," Annual forum proceedings- American Helicopter Society. Vol. 64. No. 1., 2008.
- [8] M. A. Moodie, H. Yeo, "Design of a cruise-efficient compound helicopter," Journal of the American Helicopter Society 57.3 (2012): 1-11., 2012.
- [9] G. Arnaud, and P. Beaumier, "Validation of R85/Metar on the Puma RAE Flight Tests," in *18th European Rotorcraft Forum*, 1992.
- [10] D. A. Peters, D. D. Boyd, and C. J. He, "Finite-State Induced-Flow Model for Rotors in Hover and Forward Flight," in *43rd Annual Forum of the American Helicopter Society*, 1987.
- [11] P.-M. Basset, O. Heuze, J. V. R. Prasad, and M. Hamers, "Finite State Rotor Induced Flow Model For Interferences and Ground Effect," in *57th Annual Forum of the American Helicopters Society*, 2001.
- [12] B. Benoit, A.-M. Dequin, K. Kampa, W. von Grünhagen, P.-M. Basset, and B. Gimonet, "HOST, a General Helicopter Simulation Tool for Germany and France," in *56th Annual Forum of the American Helicopters Society*, Virginia, 2000.
- [13] C. Stanger, M. Hollands, M. Kessler, and E. Krämer, "Adaptation of the Dynamic Rotor Blade Modelling in CAMRAD for Fluid-Structure Coupling within a Blade Design Process," in *18. DGLR-Fach-Symposium der STAB*, 2012.
- [14] C. B. Allen, "CHIMERA volume grid generation within the EROS code," *Proceedings of the Institution of Mechanical Engineers, Part G: Journal of Aerospace Engineering*, vol. 214, p. 125–140, 2000.
- [15] Y. Tanabe, S. Saito and H. Sugawara, "Validation of High Resolution CFD Analysis For Flowfield Around a Rotor," The 40th JSASS Annual Meeting, 2009.
- [16] C. Laurent, S. Heib and S. Plot, "The Onera elsA CFD software: input from research and feedback from industry," *Mechanics & Industry* 14.3 (2013): 159-174., 2013.
- [17] R. Jochen and J. K. Fassbender, "Block structured navier-stokes solver flower." MEGAFLOW-Numerical Flow Simulation for Aircraft Design," Springer, Berlin, Heidelberg, 2005. 27-44., 2005.
- [18] S. Yamamoto and H. Daiguji, "Higher-Order-Accurate Upwind Schemes for Solving the Compressible Euler and Navier-Stokes Equations," *Computers and Fluids*, Vol.22, Nos.2-3, pp.259-270, 1993.
- [19] K. Kitamura, and E. Shima, "Towards shock-stable and accurate hypersonic

- heating computations: A new pressure flux for AUSM-family schemes," *Journal of Computational Physics*, vol. 245, p. 62–83, 2013.
- [20] A. Jameson, W. Schmidt, and E. Turkel, "Numerical Solution of the Euler Equations by Finite Volume Methods Using Runge-Kutta Time-Stepping Schemes," in *14th AIAA Fluid and Plasma Dynamics Conference*, 1981.
- [21] G. Wilke, "New Results in Numerical and Experimental Fluid Mechanics," 1 ed., vol. XIII, Springer International Publishing, 2022, p. 790.
- [22] S. Yoon, and A. Jameson, "Lower-upper Symmetric-Gauss-Seidel method for the Euler and Navier-Stokes equations," *AIAA Journal*, vol. 26, p. 1025–1026, 1988.
- [23] S. Yoon , A. Jameson, "An LU-SSOR Scheme for the Euler and Navier-Stokes Equations," AIAA-1987-600, 1987.
- [24] S. Allmaras, F. T. Johnson, and P. Spalart, "Modifications and clarifications for the implementation of the Spalart-Allmaras turbulence model," in *Seventh International Conference on Computational Fluid Dynamics (ICCFD7)*, Big, 2012.
- [25] J. Dacles-Mariani, D. Kwak, and G. Zilliac, "On numerical errors and turbulence modeling in tip vortex flow prediction," *International Journal for Numerical Methods in Fluids*, vol. 30, p. 65–82, 1999.
- [26] J. C. Kok, "Resolving the Dependence on Freestream Values for the k- Turbulence Model," *AIAA Journal*, vol. 38, p. 1292–1295, 2000.
- [27] M. L. Shur, P. R. Spalart, M. Kh. Strelets, and A. K. Travin, "A hybrid RANS-LES approach with delayed-DES and wall-modelled LES capabilities," *International Journal of Heat and Fluid Flow*, vol. 29, p. 1638–1649, 2008.
- [28] C. C. Heister, "A Method for Approximate Prediction of Laminar-Turbulent Transition on Helicopter Rotors," *Journal of the American Helicopter Society*, vol. 63, p. 1–14, 7 2018.
- [29] D. R. Jones, M. Schonlau, and W. J. Welch, "Efficient Global Optimization of Expensive Black-Box Functions," *Journal of Global Optimization*, vol. 13, p. 455–492, 1998.
- [30] P. M. Küfmann, R. Bartels, B. G. Van_Der_Wall, O. Schneider, H. Holthusen and J. Gomes, "The first wind tunnel test of the multiple swashplate system: tesdure and principal results," *Journal of the American Helicopter Society* 62.4 (2017): 1-13., 2017.
- [31] Y. Tanabe and S. Saito, "Significance of All-Speed Scheme in Application to Rotorcraft CFD Simulations," 3rd International Basic Research Conference on Rotorcraft Technology, Nanjing, China, October 14-16, 2009.